Molecular hydrogen in the cosmic recombination epoch

Esfandiar Alizadeh and Christopher M. Hirata

Molecular hydrogen in the cosmic recombination epoch

Esfandiar Alizadeh[1, *] and Christopher M. Hirata[2, †]

[1]*Department of Physics, University of Illinois at Urbana-Champaign, 1110 West Green Street, Urbana, IL 61801*

[2]*Caltech M/C 350-17, Pasadena, CA 91125, USA*

(Dated: December 9, 2010)

The advent of precise measurements of the cosmic microwave background (CMB) anisotropies has motivated correspondingly precise calculations of the cosmic recombination history. Cosmic recombination proceeds far out of equilibrium because of a "bottleneck" at the $n = 2$ level of hydrogen: atoms can only reach the ground state via slow processes: two-photon decay or Lyman-α resonance escape. However, even a small primordial abundance of molecules could have a large effect on the interline opacity in the recombination epoch and lead to an additional route for hydrogen recombination. Therefore, this paper computes the abundance of the H_2 molecule during the cosmic recombination epoch. Hydrogen molecules in the ground electronic levels $X^1\Sigma_g^+$ can either form from the excited H_2 electronic levels $B^1\Sigma_u^+$ and $C^1\Pi_u$ or through the charged particles H_2^+, HeH^+ and H^-. We follow the transitions among all of these species, resolving the rotational and vibrational sub-levels. Since the energies of the $X^1\Sigma_g^+$–$B^1\Sigma_u^+$ (Lyman band) and $X^1\Sigma_g^+$–$C^1\Pi_u$ (Werner band) transitions are near the Lyman-α energy, the distortion of the CMB spectrum caused by escaped H Lyman-line photons accelerates both the formation and the destruction of H_2 due to this channel relative to the thermal rates. This causes the populations of H_2 molecules in $X^1\Sigma_g^+$ energy levels to deviate from their thermal equilibrium abundances. We find that the resulting H_2 abundance is 10^{-17} at $z = 1200$ and 10^{-13} at $z = 800$, which is too small to have any significant influence on the recombination history.

I. INTRODUCTION

The era of percent-level precision cosmology started with the exquisite measurements of the cosmic microwave background (CMB) anisotropies by the *Wilkinson Microwave Anisotropy Probe* (*WMAP*) satellite [1]. The CMB anisotropies are a very useful tool for cosmologists for two reasons. First, the shapes and normalizations of the temperature and polarization spectra are sensitive to a host of cosmological parameters [2]. Second, the physics underlying the CMB power spectrum is thought to be well understood. It can be calculated by linear perturbation theory of the Einstein and Boltzmann equations around a homogeneous, isotropic background [3–5]; the perturbation equations can be solved rapidly by modern numerical codes that have achieved agreement at the 0.1% level in code comparisons [6]. However, to solve these equations one needs to know the number density of free electrons as a function of redshift $n_e(z)$, the so called recombination history, which enters into these equations through the Thompson scattering of photons from free electrons.

The first cosmological recombination calculations were carried out more than 40 years ago [7, 8], showing the importance of non-equilibrium hydrogen recombination because of the high optical depth of the Lyman series lines in the early universe. A hydrogen atom can only reach its ground state from the H I 2s level or 2p levels via two-photon decay and redshifting out of the Lyman-α line, respectively. The early analyses assumed Boltzmann equilibrium of all $n \geq 2$ levels of hydrogen, and thus had to follow only ionized hydrogen $H^+ + e^-$, excited hydrogen $H^*(n \geq 2)$, and ground-state hydrogen H(1s).

To obtain $n_e(z)$ to high accuracy, it is necessary to include additional physics. Thus theorists have considered helium recombination [9–18]; deviations from Boltzmann equilibrium for the $n \geq 2$ levels of hydrogen [19–23]; a host of two-photon processes [12, 15, 24–29]; the transport of photons near Lyman-α due to multiple resonant scattering [29–37]; and cross-talk among various lines and the photoionization continuum [14, 38, 39].

The workhorse recombination code RECFAST, used for *WMAP* parameter constraints, was a fitting function to such non-equilibrium calculations including all of the physical processes recognized as important in the year $\sim$2000 [40, 41], and there have been some subsequent updates [42]. RECFAST was sufficiently accurate for the observations of its time, however to fully take advantage of the power of the *Planck* satellite data (launched 2009) it is important to find $n_e(z)$ to the sub-percent level [42, 43]. This realization triggered a flurry of papers considering a host of new phenomena that could affect the recombination history to the percent and sub-percent level, culminating in two new publicly available codes that properly treat the radiative transfer effects in hydrogen and helium recombination [44, 45].

The current paper is a continuation of the same effort to reach the required level of accuracy. We consider how the formation and destruction of hydrogen

---

*Electronic address: ealizad2@illinois.edu

†Electronic address: chirata@tapir.caltech.edu

molecules (H_2) in the $X^1\Sigma_g^+$, $B^1\Sigma_u^+$ and $C^1\Pi_u$ electronic states can change the recombination history (see Appendix A for the explanation of molecular term symbols). The reason that H_2 might be able to change the recombination history is that the Lyman and Werner bands ($X^1\Sigma_g^+$–$B^1\Sigma_u^+$ and $X^1\Sigma_g^+$–$C^1\Pi_u$) are near the Lyman-α energy ($h\nu_{Ly\alpha} = 10.2\,\text{eV}$). Thus the excitation, de-excitation, photodissociation, and photoassociation of the H_2 molecule can shuffle photons between the red and the blue sides of the Lyman-α line. In an expanding Universe, a photon redder than Lyman-α is likely to simply redshift and eventually become a part of the far-infrared background, whereas a photon bluer than Lyman-α will redshift into the Lyman-α frequency and excite a ground-state hydrogen atom (which at $z > 900$ would have been likely to be photoionized).

To assess how much effect this mechanism can have on the hydrogen atom abundance we do an order of magnitude calculation. The rate of absorption of photons by a single H_2 molecule is $n_\gamma \sigma c$, where $\sigma \sim 10^{-18}$ cm^2 is the average photon absorption cross section over the Lyman-Werner band region and c is the velocity of light. Also, n_γ is the number density of distortion photons, i.e. photons that are in excess of the black-body spectrum, because in thermal equilibrium the rate of absorption and emission of photons in any given line must be equal according to detailed balance, so only distortion photons can cause a net absorption rate. The total number of photons absorbed per unit volume by H_2 molecules during the recombination era per hydrogen nucleus is then $\sim \frac{n_{H_2} n_\gamma \sigma c \Delta t}{n_H}$. Here, $\Delta t \approx \Delta \ln(a)/H \sim 10^{13}$ sec is the duration of recombination, where a is the scale factor and H is the Hubble parameter around the recombination era. Since most of the distortion photons come from hydrogen recombination $n_\gamma \sim n_H$. The change in the ground state abundance of atomic hydrogen due to this effect, taking $n_H \sim 400$ cm^{-3} in the recombination era, is then $\Delta x_{HI} \sim 10^8 x[H_2]$. So, even a tiny quantity of molecular hydrogen can have a noticeable effect on the recombination history. It is worth noting that some models of early Universe chemistry have found $x[H_2] \gtrsim 10^{-12}$ [46, 47] during the recombination epoch with simplified (i.e. not level-resolved) reaction networks.

The calculation of the abundance of hydrogen molecules has already been considered by many authors *but for a different cosmological goal*, that is to assess the effect of the H_2 molecule on the cooling of metal-free gas and its implications for primordial star formation [48–56]. Since direct radiative association to the $X^1\Sigma_g^+$ electronic level, i.e. $2H \rightarrow H_2(X^1\Sigma_g^+) + \gamma$ is forbidden, two separate hydrogen atoms must reach the ground state of H_2 through an intermediate route. For the case of the post-recombination era when $k_B T_{CMB} < 0.2\,\text{eV}$ the accessible routes are through the H_2^+ [48] and H^- [49, 50] intermediate states. Indeed, complex reaction networks have been constructed to follow hydrogen chemistry [46, 53, 57–60]. These have identified in particular the significance of the recombination-induced CMB spectral distortion

[17, 61, 62] in controlling pregalactic photochemistry, the importance of rate coefficients [63–65], and the importance of following transitions among the various rotational and vibrational levels of the H_2^+ ion at $z < 500$ [60].

However, at the redshift of interest for this paper, $z \sim 1000$, there is another route for the formation of hydrogen molecules: the inverse Solomon process [66]. At this era there are enough ultraviolet photons (both blackbody photons and spectral distortion photons) to facilitate the photo-attachment of two hydrogen atoms into an excited H_2 molecule in one of the rovibrational levels of either the $B^1\Sigma_u^+$ (Lyman band) or $C^1\Pi_u$ (Werner band) electronic states with energies $\sim 10\,\text{eV}$. The excited H_2 molecule will re-emit the photon and decay to either a bound $H_2(X^1\Sigma_g^+)$ molecule, or to the continuum of the X level (i.e. to two H atoms). In equation form,

$$2H + \gamma \leftrightarrow H_2(B^1\Sigma_u^+, C^1\Pi_u) \leftrightarrow H_2(X^1\Sigma_g^+) + \gamma. \quad (1)$$
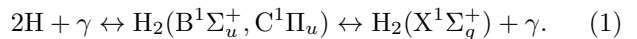
This mechanism and the charged-particle processes (H^-, H_2^+, and HeH^+) control the H_2 abundance at high redshift. The possible effect on hydrogen atom recombination is the main focus of this paper. We note that Ref. [66] found only a small production of H_2 via this mechanism, but they did not include the spectral distortion photons in their rate coefficient and hence the *total* rate of H_2 production could be many orders of magnitude larger. Of course, the same spectral distortion also drives H_2 photodissociation – the left arrows in Eq. (1) – so the net effect on the H_2 abundance requires a detailed calculation. Deviations from thermal equilibrium abundances arise not from the amplitude of the ultraviolet photon spectrum, but the way in which its peculiar shape beats against the forest of H_2 lines and dissociation continua. Since we work at $z > 800$ we will not distinguish the matter versus radiation temperature in this paper.

This paper is organized as follows: in Sec. II we write down the rate equations for the bound-bound and bound-free transitions. These equations are then solved in the steady state approximation and the results are presented in Sec. III. We discuss the size of the H_2 abundances found in the previous chapter on the absorption of Ly-α photons and conclude in Sec. IV.

II. ABUNDANCE CALCULATION

In the standard hydrogen recombination calculation [41] one follows the evolution of several hundred energy levels of the H I, He I, and He II atoms by including all bound-bound and bound-free transitions and treating the radiative transfer of line photons in the expanding universe using the Sobolev approximation [33, 67]. A similar treatment can be used for the H_2 molecule.

This section is organized as follows: we begin with a description of the reactions included (Sec. II A) and then turn to the rate equations (Sec. II B) and the steady-state approximation (Sec. II C). Finally, we describe our model

for the molecular data (Sec. II D) and the radiation field (Sec. II E), which is required in order to evaluate the transition rates among H_2 levels. The inclusion of the charged-particle reactions is described in Sec. II F.

A. Basic reactions

Here, we consider the ground X and the excited B and C electronic states of the hydrogen molecule. The latter are technically not bound since they can undergo spontaneous radiative dissociation, but they are long-lived. We designate them with their rotational (J) and vibrational (ν) quantum numbers; in the case of the C levels, which are Λ-doubled, it is necessary to describe the parity as either vector-like [C^+, $P = (-1)^J$] or axial [C^-, $P = -(-1)^J$]. We consider only the bound energy levels of these states up to rotational quantum number of $J = 20$.

The bound-free radiative reactions involving these levels (we do not consider the collisional reactions in this paper) are the dipole-allowed transitions,

$$H_2(B^1\Sigma_u^+) \leftrightarrow H(1s) + H(1s) + \gamma, \qquad (2)$$

and

$$H_2(C^{\pm\,1}\Pi_u) \leftrightarrow H(1s) + H(1s) + \gamma. \qquad (3)$$

The bound-bound reactions are the dipole-allowed transitions

$$H_2(B^1\Sigma_u^+) \leftrightarrow H_2(X^1\Sigma_g^+) + \gamma \qquad (4)$$

and

$$H_2(C^{\pm\,1}\Pi_u) \leftrightarrow H_2(X^1\Sigma_g^+) + \gamma, \qquad (5)$$

and the quadrupole-allowed transition,

$$H_2(X^1\Sigma_g^+, \nu J) \leftrightarrow H_2(X^1\Sigma_g^+, \nu'J') + \gamma. \qquad (6)$$

There are in principle other quadrupole-allowed transitions; however those involving the B and C electronic states will be small compared to the dipole-allowed transitions (B,C→X). We consider quadrupole transitions among the levels of the X electronic state with different rovibrational quantum numbers νJ because there are no allowed dipole decays from these levels, and hence quadrupole decay might be significant in comparison with excitation by (rare) ultraviolet photons.

We will denote the "thermal abundance" of an H_2 level by its abundance if the reaction 2H↔H_2 were in equilibrium, i.e.

$$
\begin{aligned}
x_{i,\mathrm{th}} = {} & \frac{(2J_i+1)g_e g_{\mathrm{nuc}}}{g_H^2} \left(\frac{2\pi\hbar^2}{k_B T}\frac{m[H_2]}{m_H^2}\right)^{3/2} \\
& \times e^{-[E_i - 2E_{H(1s)}]/kT} n_H x_{H(1s)}^2,
\end{aligned} \qquad (7)
$$

where g_{nuc} is the nuclear degeneracy, $g_e = 1$ is the electronic degeneracy, and $g_H = 4$ is the degeneracy of an

H atom. Note that since the early Universe is not in ionization (Saha) equilibrium, the choice of 2H↔H_2 as a reference reaction to define the thermal abundance is merely for convenience, and that achieving the thermal abundance does not imply full thermodynamic equilibrium.

B. Rate equations

The rate equations for the above reactions can be written as:

$$\dot{x}_i = \dot{x}_i|_{bb} + \dot{x}_i|_{bf}, \qquad (8)$$

where i denotes the level under consideration (we always resolve rotational and vibrational quantum numbers of H_2), the overdot $\dot{}$ denotes a derivative with respect to proper time, and $x_i \equiv n_i/n_H$ where n_H is the proper density of hydrogen nuclei (in any form – H II, H I, or H_2).

The bound-bound term is given by:

$$
\begin{aligned}
\dot{x}_i|_{bb} = {} & -\sum_{j<i} P_{ij}\left\{ x_i A_{ij}[1 + f(\nu_{ij+})] - x_j A_{ij}\frac{g_i}{g_j}f(\nu_{ij+})\right\} \\
& + \sum_{j>i} P_{ji}\left\{ x_j A_{ji}[1 + f(\nu_{ji+})] - x_i A_{ji}\frac{g_j}{g_i}f(\nu_{ji+})\right\}.
\end{aligned}
$$
$$(9)$$

The first sum in the right hand side shows the rate of decrease of x_i by radiative decays to lower levels (spontaneous + stimulated) and increase of x_i by radiative absorption. The second sum is for radiative decays from the higher levels to the level i and their inverse processes. Here $f(\nu_{ji+}) = f(\nu_{ji} + \epsilon)$ is the photon phase space density on the blue side of the line. Also, P_{ij} is the Sobolev escape probability [68] (see Ref. [41] for a short derivation) which is the probability that a photon emitted in the line to escape out of it via redshifting before being reabsorbed by a molecule in a lower j level. It is given by:

$$P_{ij} = \frac{1 - e^{-\tau_{ij}}}{\tau_{ij}}, \qquad (10)$$

where the optical depth is

$$\tau_{ij} = \frac{c^3 n_H}{8\pi H \nu_{ij}^3} A_{ij}\left(\frac{g_i}{g_j}x_j - x_i\right). \qquad (11)$$

As a first step, we assume the H_2 lines are optically thin, that is $|\tau_{ij}| \ll 1$, and therefore all the emitted photons will escape out of the resonance ($P_{ij} \approx 1$). This assumption must be checked at the end of the calculation for self-consistency; later we will find it to be extremely good for all lines.

Similarly, the bound-free term can be written as

$$\dot{x}_i|_{bf} = -x_i \int_{E_{\text{free}}}^{E_i} \alpha_i(E_f)[1 + f(E_i - E_f)]\, dE_f$$

$$+ n_{\text{H}} x_{\text{H(1s)}}^2 \int_{E_{\text{free}}}^{E_i} \beta_i(E_f) f(E_i - E_f)\, dE_f. \quad (12)$$

The first term on the right hand side is for the dissociation of the hydrogen molecule into two H(1s) atoms via radiative decay to an unbound vibrational state, and the second term is for the inverse process. Here $E_{\text{free}} = -1$ Hartree is the energy of two separated H(1s) atoms with no relative kinetic energy. The functions $\alpha_i(E) dE = A_{i \to \text{free}}(E) dE$ are the Einstein coefficients for the decay from a bound state i to the continuum with energy E. The radiative absorption coefficients β_i can then be calculated using the principle of detailed balance:

$$\beta_i(E) = \left(\frac{x_i}{n_H x_H^2}\right)_{\text{th}} \frac{1 + f_{\text{th}}(E_i - E)}{f_{\text{th}}(E_i - E)} \alpha_i(E). \quad (13)$$

Using equilibrium thermodynamics to find the thermal abundance ratio (Eq. 7) and plugging in the blackbody spectrum $f_{\text{th}}(E) = 1/(e^{E/k_B T} - 1)$ we finally find

$$\beta_i(E) = \frac{(2J_i + 1) g_e g_{\text{nuc}}}{g_{\text{H}}^2} \left(\frac{2\pi\hbar^2}{k_B T} \frac{m[\text{H}_2]}{m_{\text{H}}^2}\right)^{3/2}$$

$$\times e^{-(E_i - E_{\text{free}})/k_B T} \alpha_i(E). \quad (14)$$

Here, $g_{\text{H}} = 4$ is the degeneracy of the ground energy level of the hydrogen atom, g_e is the electron spin degeneracy of the bound state i and is equal to 1 for all the states considered in this paper as they are all in singlet electronic spin states. Finally, g_{nuc} is the nuclear spin degeneracy of the bound state i. It can be calculated by demanding that the total wavefunction change the sign under exchange of the two protons; this implies $g_{\text{nuc}} = 1$ for the even-J energy levels of the X, B and C$^+$ electronic states and for the odd-J states of C$^-$. For the rest of the bound states the protons are in their triplet spin state, i.e $g_{\text{nuc}} = 3$.

C.   Steady state approximation

We can rewrite the rate equations above in matrix form. To do that it is convenient to define the bound-bound transition matrix:

$$R_{ij} = \begin{cases} A_{ij}[1 + f(\nu_{ij})] & j < i \\ (g_j/g_i) A_{ji} f(\nu_{ij}) & i < j \\ 0 & i = j. \end{cases} \quad (15)$$

In addition, we define the dissociation term

$$\gamma_i = \int_{E_{\text{free}}}^{E_i} \alpha_i(E_f)[1 + f(E_i - E_f)]\, dE_f, \quad (16)$$

and the source term

$$s_i = \int_{E_{\text{free}}}^{E_i} n_{\text{H}} x_{\text{H(1s)}}^2 \beta_i(E_f) f(E_i - E_f)\, dE_f. \quad (17)$$

Then it is straightforward to show that the Eqs. (8), (9) and (12) can be written in the compact form

$$\dot{x}_i = -\sum_j T_{ij} x_j + s_i \quad (18)$$

where the transition matrix $\mathbf{T}$ is defined by:

$$T_{ij} = \delta_{ij}\left(\sum_k R_{ik} + \gamma_i\right) - R_{ji}. \quad (19)$$

If the transition times are much smaller than the age of the Universe, i.e. if the smallest eigenvalue $\lambda_{\min}$ of $\mathbf{T}$ is $\gg H$, we can take $\dot{x}_i = 0$. Then the abundances can be found by the solution to the linear system:

$$\mathbf{x} = \mathbf{T}^{-1}\mathbf{s}. \quad (20)$$

In fact, since the steady-state H$_2$ abundance is exponentially increasing at the end of recombination, we would like $\lambda_{\min}$ to be larger than ζH, where $\zeta = d\ln x_{\text{ss}}[\text{H}_2]/d\ln a$. The steady-state approximation is found to be valid until $z \approx 810$, i.e. during the portion of the recombination epoch most relevant to CMB anisotropies. We will find the smallest eigenvalue of $\mathbf{T}$ to become $\approx H$ at $z = 750$.

D.   Molecular data

We require the bound-bound and bound-free Einstein coefficients A_{ij} and α_i. These must be calculated since no tabulations of the full radiative dissociation spectrum from the B and C states is available (Ref. [69] gives integrated radiative dissociation rates and mean photon energies, but not a spectrum as required here).

For the energy levels and dipole transitions, we use the Born-Oppenheimer approximation. This may not be accurate for nearly degenerate vibrational levels of the B and C$^+$ states: these can mix if they have the same rotational quantum number J (C$^-$ states cannot mix with B by parity conservation). In these cases, if e.g. the decay rate to a particular X rovibrational level is much greater for the pure B than the pure C$^+$ state, then the mixing can enhance the decay rate from the energy eigenstate that is "mostly" C$^+$ [69, 70]. However, in these cases we expect that the rates involving the B state would have a greater impact on the H$_2$ abundance than the C$^+$ state. Therefore, the Born-Oppenheimer approximation is sufficient for the purpose of order-of-magnitude estimation of the H$_2$ abundance.

We have acquired the electronic energy level surfaces from the literature for the X [71], B [72] and C [73] states, and used them to construct Born-Oppenheimer
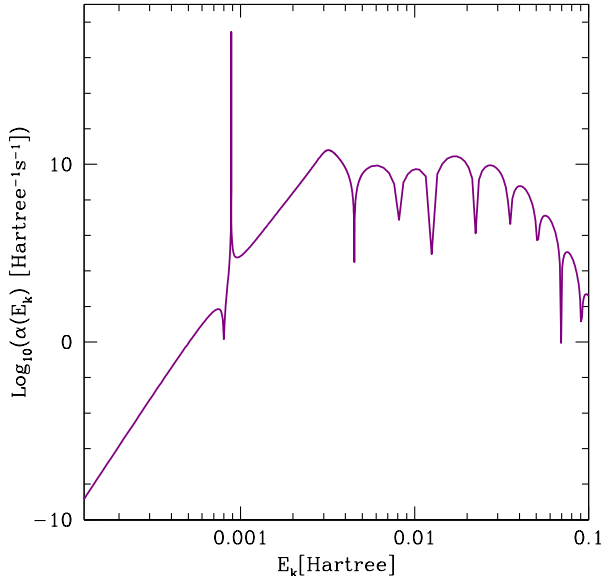
FIG. 1: The P-branch contribution to the spontaneous dissociation of $H_2(B^1\Sigma_u^+)$ from the $J = 14$, $\nu = 9$ level, as a function of the center-of-mass frame kinetic energy of the final H atoms. Note the quasibound resonance peak at $E_k = 0.0009$ Hartree, which contains $\sim 4\%$ of the integrated rate.

wave functions. The electronic dipole matrix elements have also been obtained from the literature for X–B [74] and X–C [73] transitions. (The expressions for Einstein coefficients can be found in Appendix B.) Note that for the radiative dissociation of the B and C electronic states, we consider decays to the vibrational continuum of the X electronic state.

The dissociation coefficient $\alpha_i(E_f)$ is a complicated function of the final energy E_f due to the existence of quasibound resonances of the H_2 $X^1\Sigma_g^+$ electronic state that ultimately dissociate via tunneling through the centrifugal barrier. This behavior can still be captured by the Born-Oppenheimer approximation as long as one uses sufficiently small steps in E_f; see Fig. 1. (In principle, there is an additional requirement that the resonances not be radiatively broadened, but since they have no allowed decays this is not a problem for us.) In practice, when computing the integrals in Eq. (12) we use the adaptive step size integrator `odeint` of Ref. [75].

We also consider the effect of adding the electric quadrupole transitions among different $X^1\Sigma_g^+$ states on the H_2 abundances by using the results of Ref. [76] for the corresponding Einstein coefficients.

E. Radiation field

The above equations require knowledge of the radiation field as a function of the photon energy, $f(E)$. The relevant range of energies extends up to 0.54 Hartree (14.7 eV). This includes the range in which the spectral distortion is significant. It also extends to energies greater than the ionization energy of H I, $E_I = 13.6$ eV=0.5 Hartree.

The CMB blackbody component is specified by the radiation temperature. This is $T(z) = 2.728(1 + z)$ Kelvin, and we have not distinguished between the matter temperature and the radiation temperature (in our redshift range $z > 800$ these differ by $< 0.1\%$). The number density of hydrogen nuclei is

$$n_H(z) = \frac{(1 - Y)\rho_{cr}\Omega_{b,0}}{m_p}(1 + z)^3, \tag{21}$$

where $Y = 0.24$ is the mass weighted primordial helium abundance, $\rho_{cr} = 1.8788 \times 10^{-29}h^2$ g cm^{-3} is the critical density of the universe at the present time, m_p is the proton mass and $\Omega_{b,0}h^2 = 0.022$ is the baryon density parameter at the present time.

The radiation field at $E < E_I$ is obtained using the code of Ref. [28], which includes both CMB blackbody and spectral distortions. This code self-consistently follows the absorption and emission of Lyman-series photons in the H I lines. In the case of two-photon transitions, it follows only the harder rather than the softer of the two photons. This leads to small errors at $E < \frac{3}{8}E_I$, because the lower-energy photon in the decay

$$H(2s) \leftrightarrow H(1s) + \gamma + \gamma \tag{22}$$

is ignored. However, at the redshifts of interest here ($z > 800$) this is not a significant oversight because the CMB blackbody is dominant at these low energies, and even at later times the distortion from redshifting of higher-energy photons (Lyman-α or the hard 2γ photons) is more important than the soft 2γ photons. The code also includes the spectral distortion due to two-photon decays from higher levels H(3s,3d), and due to the Raman process

$$H(2s) + \gamma \leftrightarrow H(1s) + \gamma, \tag{23}$$

which results in a significant addition to the photons at $E > E_{Ly\alpha}$.

The code of Ref. [28] does not track the extreme ultraviolet (EUV), defined here as photons energetic enough to ionize hydrogen, $E \geq E_I$. The reason is that the Universe is optically thick to such photons: in $< 10^{-7}$ Hubble times these photons will be absorbed. There is, however, a constant stream of EUV photons being produced via direct recombinations to the ground state,

$$H^+ + e^- \leftrightarrow H(1s) + \gamma_{EUV}. \tag{24}$$

The abundance of these photons will thus rapidly reach its equilibrium value [38]; in the limit of $f(E) \ll 1$ so that we can neglect stimulated recombinations, we have

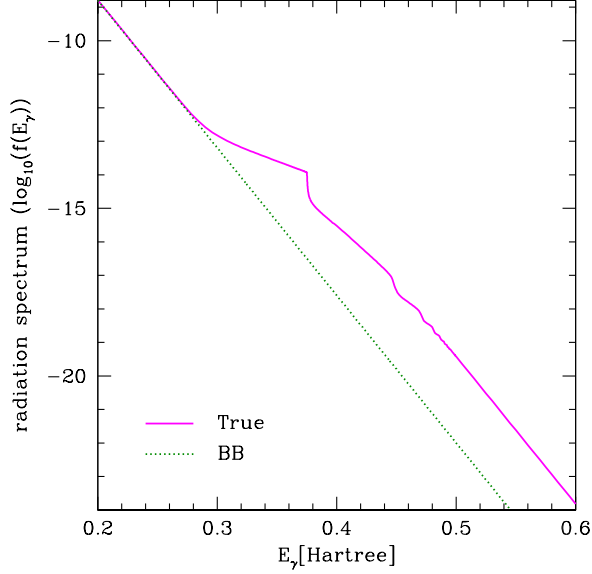$$f(E) = e^{-E/k_BT}\frac{n[H^+]n_e/n[H(1s)]}{\{n[H^+]n_e/n[H(1s)]\}_{Saha}}. \tag{25}$$

FIG. 2: The radiation spectrum at $z = 1142$, showing both the CMB blackbody spectrum (straight line) as well as the full calculation including H spectral distortions.

[The "temperature" in this equation (both in the exponential and the Saha abundance ratio) is technically the matter temperature T_{m} since the photons are being produced and destroyed by interaction with matter, but at high redshift we do not make this distinction.]

The overall radiation spectrum is shown in Fig. 2 at $z = 1142$.

In our analysis, we take the output of the standard calculation, namely the abundance of hydrogen atoms and the phase space density of photons as a function of redshift and energy, as the input in our calculation of the abundance of hydrogen molecule levels. Of course, if H_2 abundances turn out to be high enough to make a considerable change in the recombination history or radiation spectrum, one must perform a more self-consistent calculation in which the feedback of H_2 molecules on hydrogen recombination is taken into account properly by solving the rate equation for all of the species simultaneously. But for the standard cosmology, we will see that this situation does not arise.

F. The charged-particle processes

We have investigated the processes that produce H_2 from neutral hydrogen atoms and radiation. However, there are other mechanisms that contribute to their formation and destruction, namely the H^-, H_2^+, and HeH^+ pathways (these have been found to be dominant at low z in previous works, e.g. Refs. [46, 60]).

All of the reactions that we consider in this paper, including these pathways, are shown in Fig. 3. They
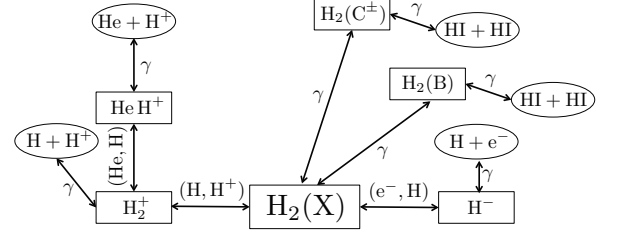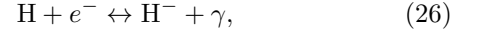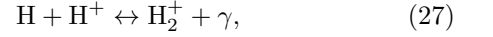

FIG. 3: The network of routes for the formation and destruction of an H_2 molecule that we consider in this paper.

include the radiative attachment/detachment for H^-
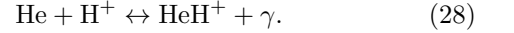
$$H + e^- \leftrightarrow H^- + \gamma, \tag{26}$$

the radiative association/dissociation of H_2^+

$$H + H^+ \leftrightarrow H_2^+ + \gamma, \tag{27}$$

and that for HeH^+

$$He + H^+ \leftrightarrow HeH^+ + \gamma. \tag{28}$$
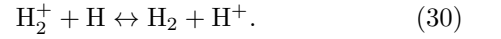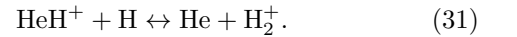
There are subsequent nonradiative reactions that generate H_2 (and at sufficient temperature can destroy it by operating in reverse): the H^- channel

$$H^- + H \leftrightarrow H_2 + e^- \tag{29}$$

and the H_2^+ channel

$$H_2^+ + H \leftrightarrow H_2 + H^+. \tag{30}$$

The latter can be aided by proton exchange from HeH^+:

$$HeH^+ + H \leftrightarrow He + H_2^+. \tag{31}$$

1. Positive channel: H_2^+ and HeH^+

The positive ion channel (H_2^+) must be treated via level-resolved chemistry [46, 59, 60]. Our solution to this is to extend the **T**-matrix to include the additional species. That is, we write

$$\mathbf{T} = \begin{pmatrix} \mathbf{T}_{H_2,H_2} & \mathbf{T}_{H_2,H_2^+} & \mathbf{T}_{H_2,HeH^+} \\ \mathbf{T}_{H_2^+,H_2} & \mathbf{T}_{H_2^+,H_2^+} & \mathbf{T}_{H_2^+,HeH^+} \\ \mathbf{T}_{HeH^+,H_2} & \mathbf{T}_{HeH^+,H_2^+} & \mathbf{T}_{HeH^+,HeH^+} \end{pmatrix}, \tag{32}$$

and similarly the source vector $\mathbf{s}$ and abundance vector $\mathbf{x}$ are extended. The model H_2 molecule includes 1435 levels (X, B, C^+, C^-) with $J \leq 20$. We follow all 423 rovibrational levels of $H_2^+(X^2\Sigma_g^+)$. However, we treat the $HeH^+(X^1\Sigma^+)$ ion assuming Boltzmann distribution of the rovibrational levels at the radiation temperature,

which is a good approximation since electric dipole transitions are allowed and rapidly thermalize the level populations. The full **T**-matrix is thus 1859×1859.

The sub-block of the **T**-matrix and **s**-vector involving H_2^+ and HeH^+ was computed in Ref. [60]: it contains Eqs. (27), (28), and (31), as well as contributions associated with the electric quadrupole transitions among the rovibrational states of $H_2^+(X^2\Sigma_g^+)$. We used the code and rate coefficients of Ref. [60] to generate the corresponding matrices and source vectors. Since none of our reactions directly connect HeH^+ to H_2 (they can only interconvert via H_2^+), we set $\mathbf{T}_{H_2,HeH^+} = \mathbf{0}$ and $\mathbf{T}_{HeH^+,H_2} = \mathbf{0}$. It therefore remains only to determine the sub-blocks $\mathbf{T}_{H_2,H_2^+}$ and $\mathbf{T}_{H_2^+,H_2}$, which arise from Eq. (30). These are related by the usual detailed balance relation,

$$\frac{R_{ji}}{R_{ij}} = \frac{x_{i,\text{th}}}{x_{j,\text{th}}} = \frac{x[H(1s)]}{x[H^+]} \frac{g_i}{2g_j} e^{(E_j + E_{H(1s)} - E_i - E_{H^+})/k_B T},$$
(33)

where i represents any state of H_2, j any state of H_2^+, $E_{H(1s)} - E_{H^+} = -13.6$ eV, and the factor of 2 comes from the degeneracy ratio of H versus H^+. The corresponding contributions to **T** can then be determined from Eq. (19).

The rovibrational level-resolved forward reaction rates R_{ij} for Eq. (30) are unfortunately not available in the literature. Vibrationally resolved quantum-mechanical rates have been calculated [77], however their calculation did not resolve the rotational levels and did not well-sample the lowest energies required here. There is also the experimentally measured low-temperature rate of 6.4×10^{-10} cm^3 s^{-1} [78], which once again did not resolve rovibrational levels (see also the recent measurements of the reaction of D_2^++H [79]). The experiment of Ref. [78] did however show by isotopic substitution that the reaction mechanism is charge transfer, i.e. the two nuclei in the initial H_2^+ ion remain in the H_2 molecule that is produced. Therefore the ortho- or para- nuclear spin character should be preserved in the reaction of Eq. (30).

Since the calculations of Ref. [77] suggest that at energies of several tenths of an eV the reaction $H_2^+(\nu = 0)$+H→H_2+H^+ is most likely to leave the final molecule in the $\nu = 4$ vibrational state, a simple prescription is to assume that (i) the rate coefficient for this reaction is 6.4×10^{-10} cm^3 s^{-1}; (ii) the final vibrational state is $\nu = 4$; and (iii) the rotational quantum number (N for H_2^+ and J for H_2) is unchanged in the collision.

2. Negative channel: H^-

Previous work [46, 59, 60] has established that at $z > 200$, reaction Eq. (26) forces the H^- abundance to its thermal equilibrium value because (i) the matter and radiation temperatures are equal, and (ii) photodetachment by blackbody photons is the main sink for H^- on account of the strong CMB field and the low binding energy of H^-, $B[H^-] = 0.754$ eV. The thermal abundance

is then given by

$$x[H^-] = \frac{n_H x_e x_{H(1s)}}{4} \left(\frac{2\pi\hbar^2}{m_e k_B T} \right)^{3/2} e^{B[H^-]/k_B T}. \quad (34)$$

The associative detachment reaction, Eq. (29), can be incorporated by adding appropriate sources and sinks. For the sources, we add

$$s_i + = k_i n_H x[H^-] x[H(1s)], \quad (35)$$

where "+ =" means that the quantity is added to s_i. Here k_i is the rate coefficient to level i of H_2, which we obtain from the calculations of Ref. [80]; we use the $T = 3000$ K column of their table as it is most appropriate for the recombination epoch and the temperature dependences are weak. Detailed balance implies a corresponding sink for H_2 molecules:

$$T_{ii} + = \frac{k_i n_H x[H^-] x[H(1s)]}{x_{i,\text{th}}}. \quad (36)$$

(We may use $x_{i,\text{th}}$ here since the negative species are catalysts and hence have no effect if H_2 is at the thermal abundance; one may check explicitly that T_{ii} in fact is proportional to $n_{H(1s)}$ with a coefficient that depends only on temperature.)

III. RESULTS

A. H_2 abundance

We now determine the H_2 abundance by two methods: first, with only the Lyman and Werner band reactions as sources and sinks for H_2; and second, including the charged particle reactions as well. The latter, of course, is our final result.

1. H_2 dipole and quadrupole transitions only

The abundances of the H_2 molecule in different rovibrational states x_i can be found by using Eqs. (14–20).

The total abundance of *all* H_2 molecules irrespective of rovibrational state is shown in Fig. 4. This abundance shows the expected rapid increase in the early stages of recombination as the temperature drops. At $z \lesssim 1400$, the photon phase space density $f(E)$ begins to deviate substantially from the Planck spectrum. One can see that the sense of the resulting spectral distortion is a temporary *decline* in the abundance of H_2, followed by a rapid recovery as the spectral distortion redshifts below the Lyman-Werner bands.

We show in Fig. 5 the ratio $x_i/x_{i,\text{th}}$ of the abundances of the states in all vibrational levels within the $X^1\Sigma_g^+$ $J = 0$ sequence of the hydrogen molecule to their abundances in thermal equilibrium at $z = 1142$. Here again "equilibrium" refers to the abundance $x_{i,\text{th}}$ that would be

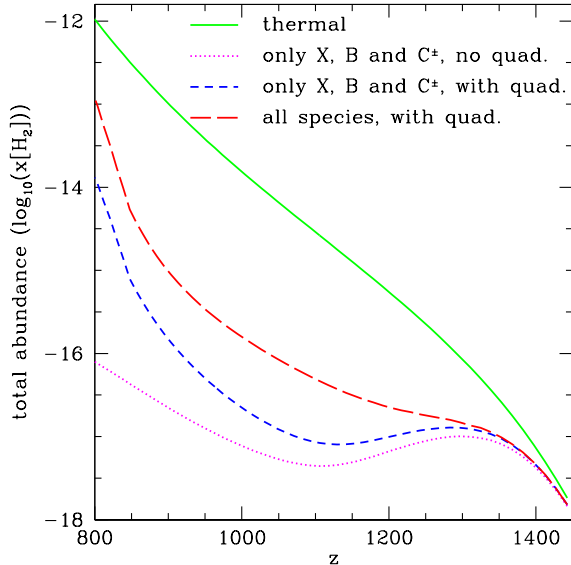FIG. 4: The abundance of H_2 molecules, $x[H_2]$, as a function of redshift. Short dashed blue and dotted magenta lines show the cases where we do and do not include quadrupole transitions between X levels, respectively, and only the Lyman and Werner band reactions can create and destroy H_2. The long dashed red curve shows the case when all the relevant reactions are included. The green solid curve shows the thermal abundances of Eq. (7).

FIG. 5: The ratios of the abundances of the H_2 $X^1\Sigma_g^+$ levels with $J = 0$ to their thermal values at $z = 1142$, plotted as a function of the vibrational quantum number ν. Blue stars and magenta squares show the cases with and without quadrupole transitions between the X electronic levels, respectively. This plot included only the Lyman and Werner band reactions as sources and sinks for H_2.

obtained if the reaction $H_2(X^1\Sigma_g^+, \nu, J) \leftrightarrow 2H(1s)$ were in equilibrium at the *actual* H(1s) abundance (the definition is important since the ionization fraction deviates from Saha). The first two vibrational levels have approximately the same $x_i/x_{i,\text{th}}$; then there is a sudden drop in this ratio going from the second to the third vibrational level, after which $x_i/x_{i,\text{th}}$ increases steadily and approaches 1 for the weakly bound states. The physical reason for this situation is that a photon in or redward of the H I Lyman-α line is capable of exciting an H_2 molecule only from the $\nu \geq 2$ vibrational levels (starting from $\nu = 0, 1$ there is insufficient energy to reach the B or C electronic states). Thus the $\nu \geq 2$ vibrational levels are rapidly photodissociated. The inclusion of the quadrupole transitions enables $H_2(X^1\Sigma_g^+)$ molecules to switch among the various vibrational levels and leads to a washing-out of the step in abundance versus ν.

2. Inclusion of charged particle reactions: H_2^+, HeH^+, and H^-

We now turn on our full reaction network. We display the abundances of the various levels of H_2 by plotting the logarithmic abundance $\log_{10}(x_i/g_i)$ versus the level energy. This is a straight line in the case of a thermal distribution of levels. The actual result is shown in Fig. 6 for the X electronic states on the left and the B, C^+ and
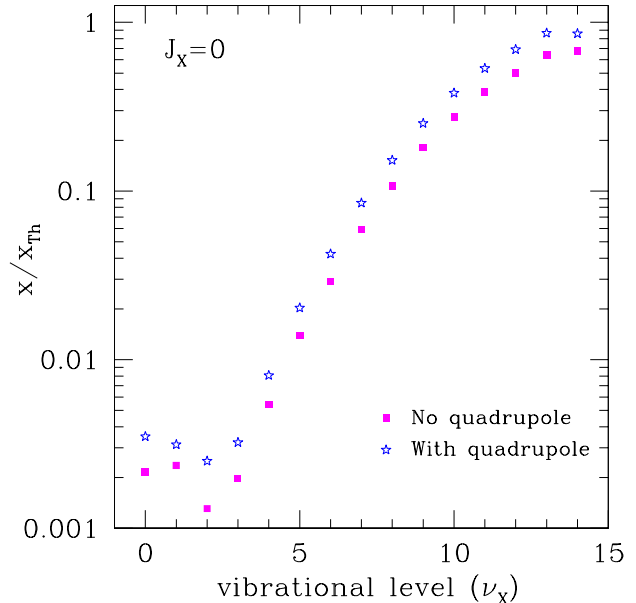
C^- on the right. We can see that the highly excited rovibrational levels of the X electronic state are near thermal equilibrium, but the lower levels are underpopulated by ~ 2 orders of magnitude. On the other hand the B, C^+ and C^- states are overpopulated compared to the equilibrium abundance and they become more overpopulated relative to thermal for higher energy levels. This is a consequence of the shape of the spectral distortion.

Thus far we have assumed the steady state approximation, i.e. that all of the eigenvalues of the **T**-matrix are large compared to the Hubble expansion rate H. The minimum eigenvalue of **T** is shown in Fig. 7 together with the Hubble rate. We can see that for $z > 800$ the minimum eigenvalue λ_{min} is much larger than the Hubble rate. In fact, due to the rapid increase in the H_2 abundance, we should really be comparing λ_{min} to $d \ln x[H_2]/dt$; the crossing of these occurs at $z \approx 810$, which is roughly where we expect the steady state approximation to fail. As a consequence, we do not show H_2 abundances at lower redshifts.

In Fig. 4 we show the sum of the abundances of all the X, B and $C^\pm$ levels of the H_2 molecule as a function of redshift (in practice, this sum is dominated by the X electronic state). Short dashed blue and dotted magenta lines show the cases where we do and do not include quadrupole transitions between X levels, respectively, and only the Lyman and Werner band reactions can cre-
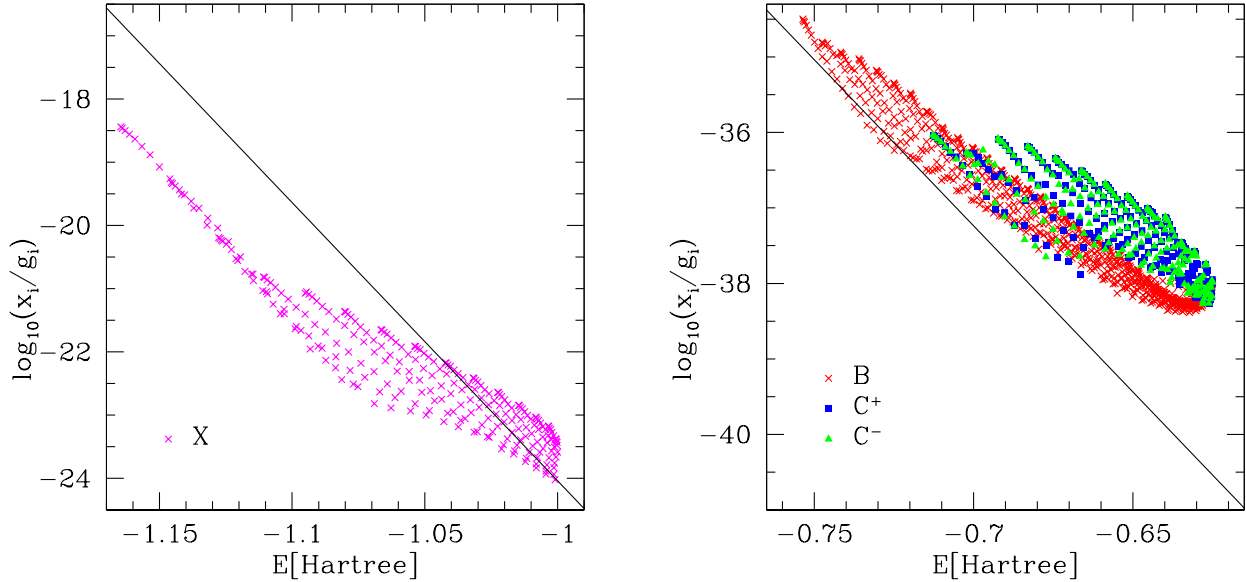
FIG. 6: The abundance of each H_2 level plotted versus the level energy at $z = 1142$. In the left panel we show the abundances of X levels and in the right panel the B, C^+ and C^- levels. The solid line shows the thermal equilibrium abundances.
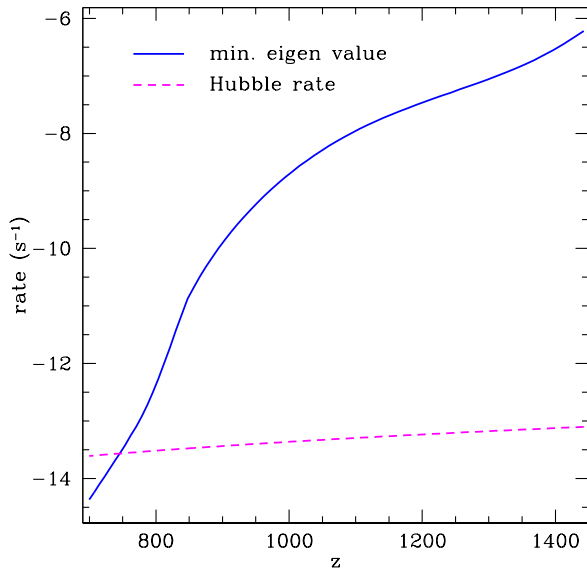

FIG. 7: The minimum eigenvalue of the rate matrix T (solid blue) as compared to the Hubble rate (dashed magenta).

ate and destroy H_2. The long dashed red curve shows the case when all the relevant reactions are included. The green solid curve shows the thermal abundances of Eq. (7). We can see that the addition of new transitions consistently causes the non-thermal abundance of H_2 molecules to increase, while always staying below the thermal abundance.

We also show the abundances of the intermediate species in Fig. 8. The left panel shows the abundances of the charged particles and the right panel the excited electronic states B and $C^{\pm}$ of the hydrogen molecule. Even though the abundances of the excited states are much smaller than those of the charged particles, they must be included since the transition rates between these excited states and the H_2 ground state can be much higher than the transition rates connecting the charged particles to the ground state.

A related possible formation channel for H_2 that is mentioned in the literature is from the reaction of an excited and a ground-state H atom [66]:

$$H(1s) + H(n = 2) \leftrightarrow H_2(X^1\Sigma_g^+) + \gamma. \qquad (37)$$
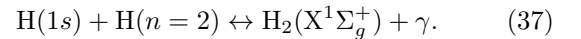
This reaction proceeds if the reactants approach each other in the vibrational continuum of a $^1\Sigma_u^+$ or $^1\Pi_u$ electronic state (usually B or C), and in order to produce a bound H_2 molecule the photon must have an energy $E > E(\text{Ly}\alpha)$. Since the phase space density of photons is a steeply decreasing function of energy (including a step at Lyman-α), we would expect that the photodissociation of the levels of H_2 is dominated by transitions through the discrete vibrational levels of $B^1\Sigma_u^+$ and $C^1\Pi_u$ rather than the higher-energy continuum. One can also check the formation of H_2 by this mechanism directly: using the rate coefficient $2.09 \times 10^{-14}(T/300\,\text{K})^{0.24}e^{-T/37800\,\text{K}}$ cm^3 s^{-1} [57], we find a maximum production rate of H_2 molecules per H nucleus per Hubble time of 7×10^{-12} at $z = 1250$. This channel is thus subdominant to the HeH^+/H_2^+ channel. All of these are small compared to the transitions through $H_2(B^1\Sigma_u^+, C^1\Pi_u)$.
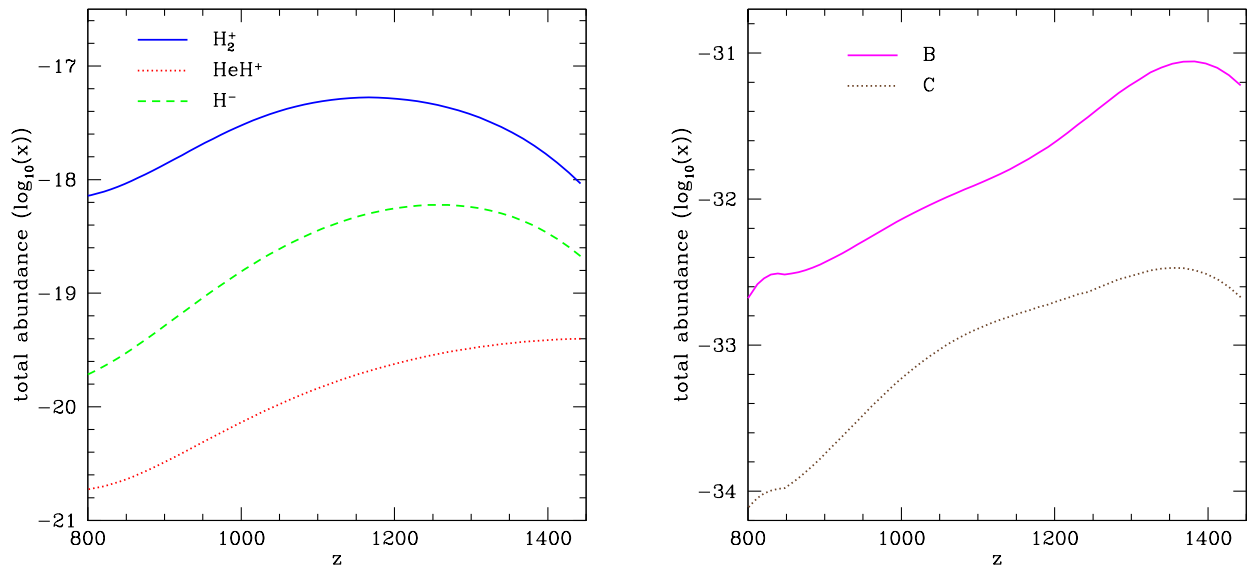
FIG. 8: Here we show the abundances of the intermediate species, H^-, H_2^+, and HeH^+ in the left panel and $H_2(B,C^\pm)$ in the right panel, as a function of redshift during the recombination epoch.

B. Effect on recombination

Since some of the X–B and X–C transitions have energy above the Lyman-α energy, the absorption or emission of a photon in this line by an H_2 molecule adds or removes a photon that would have otherwise excited a hydrogen atom at a later time, and therefore it will alter the process of recombination of hydrogen atoms. To estimate this effect, we must estimate both the Sobolev optical depth of the various lines using Eq. (11), and the rate of production of photons in the X–B and X–C bands.

In Fig. 9 we show the net Sobolev optical depth for all X–B and X–C lines. We can see that the optical depth of the sum of all the lines is much smaller than one, and therefore each individual line is also optically thin. This then justifies using $P_{ij} = 1$ for the Sobolev escape probability throughout this paper.

The net rate of emission of photons in the X–B and X–C bands at energies above the Lyman-α energy is shown in Fig. 10. We see that there was no absorption or emission in this line at very early times when the universe was in thermal equilibrium. However, at redshifts of ~ 1500 the deviation of the hydrogen molecule abundances from their thermal values, coupled with the CMB spectral distortion, lead to a net emission of super Lyα photons for both the Lyman and Werner bands. The Lyman band, however, started absorbing super Lyα radiation later on. The net number of emitted photons turns out to be negligible ($\sim 10^{-11}$) and so it can only cause a very small change in the abundance of H atoms.

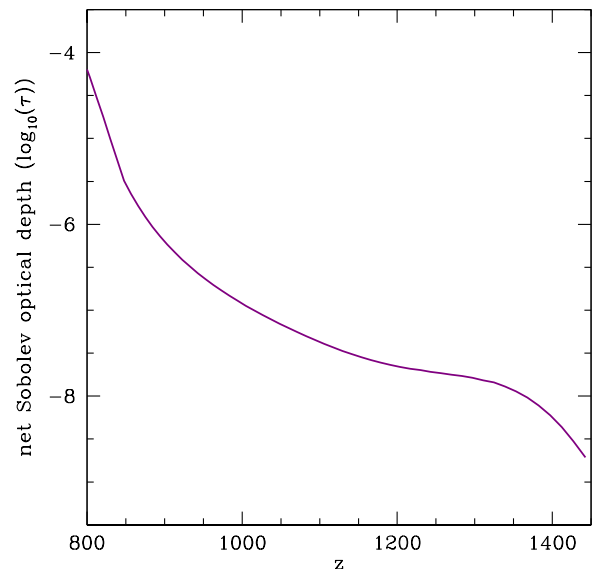There is one final possibility for reactions involving H^- and H_2^+ to affect recombination, namely through the neu-

FIG. 9: Total Sobolev optical depth of all of the Lyman and Werner lines as a function of redshift.

tralization reactions

$$H^- + H^+ \leftrightarrow 2H \qquad (38)$$

and

$$H_2^+ + e^- \leftrightarrow 2H, \qquad (39)$$

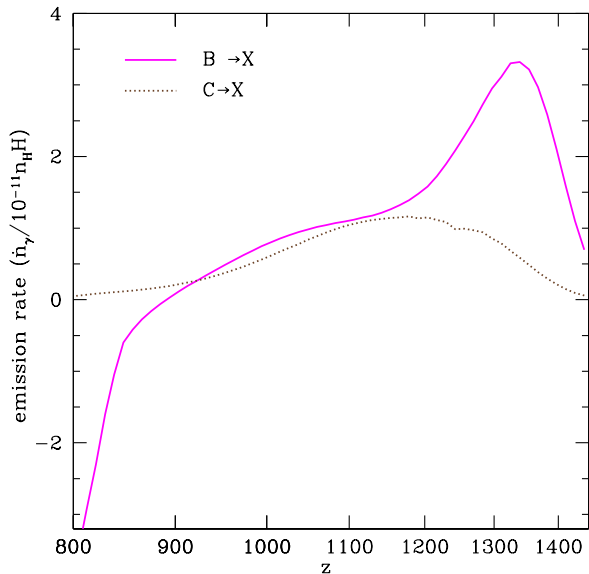which – in combination with Eqs. (26) and (27) – lead to a net recombination. They are, however, negligible:

FIG. 10: The net rate of emission (i.e. emission minus absorption) of photons at $E > E(\text{Ly}\alpha)$ in the H_2 Lyman and Werner bands, measured in photons per H nucleus per Hubble time.

even for the "upper limit" rate coefficient for Eq. (38) of 5×10^{-9} cm^3 s^{-1} [63], we obtain a maximum recombination rate per Hubble time ($\dot{x}_{1s}/H$) of 1.1×10^{-11}. Even this is too large since Eq. (38) usually leaves one of the hydrogen atoms in an excited level (principally $n = 3$) [81] from which it has a large probability of being photoionized. Similarly, for Eq. (39), the rate coefficient at recombination-epoch temperatures is of order $\sim 10^{-8}$ cm^3 s^{-1} [82], which implies recombination rates $\dot{x}_{1s}/H$ of order 10^{-10}.

IV. DISCUSSION AND CONCLUSION

Since the Lyman and Werner band transition energies of H_2 are near the H Lyα energy, it is expected that the abundances of H_2 energy levels deviate appreciably from their thermal abundances. This is because the photon phase space density has been distorted by the redshifted Lyα photons as in the standard hydrogen atom recombination picture. However, it is not clear from the outset whether this distortion to the photon phase space density increases or decreases the abundances of H_2 levels compared to their thermal abundances, since the spectral distortion photons accelerate both the production and destruction of H_2. To answer this question and ultimately to see to what extent the H_2 molecules can affect the recombination history we have in this paper carried out a detailed calculation including all of the rovibrational levels of the H_2 $X^1\Sigma_g^+$, $B^1\Sigma_u^+$, and $C^1\Pi_u$ electronic states up to rotational number $J = 20$, together with the

charged species relevant to the formation of hydrogen molecules, that is H_2^+, HeH$^+$ and H$^-$. We have calculated the bound-bound and bound-free dipole transition rates for the Lyman and Werner bands of the hydrogen molecule using the Born-Oppenheimer approximation. Special care has been taken to find the resonances of the bound-free transitions. The rate equations connecting the energy levels are then solved in the steady state approximation and the level abundances are found by a matrix inversion for each given redshift.

The main result of our paper is that the shape of the CMB spectral distortion reduces the abundance of H_2 compared to the thermal abundance, resulting in low H_2 abundances throughout the recombination epoch; see Fig. 4. The inclusion of the quadrupole transitions among rovibrational levels of the X electronic state increases the H_2 abundance, and adding the charged particle processes increases the H_2 abundances yet more, while remaining below the thermal abundance. We find $x[H_2] \sim 10^{-16}$ during most of the recombination epoch, rising to 10^{-13} at $z = 800$. We conclude that – despite the high cross section for Lyman and Werner band absorption – H_2 is not relevant for determination of the primordial recombination history and CMB anisotropies.

Appendix A: Molecular Term Symbols

Like the atomic term symbols, the molecular term symbols are a convenient and concise way of writing the symmetries and the angular momentum properties of the *electronic* part of the wavefunction of a molecule. In the case of a linear molecule, and ignoring the spin-orbit couplings, the electronic angular momentum operators that commute with each other and with the electronic Hamiltonian are $(\hat{S}^2, \hat{S}_z, \hat{L}_z)$, where z-axis is along the internuclear axis of the molecule. For homonuclear diatomic molecule, which is the case we are dealing with, the term symbol is conventionally written as

$$^{2S+1}\Lambda_{g/u}^{(+/-)} \tag{A1}$$

where S is the quantum number for the total spin operator $\hat{S}^2$, Λ is the absolute value of the eigenvalue of the projection of the orbital angular momentum along the internuclear axis, $\hat{L}_z$. Different values of Λ are commonly

shown by Σ, Π, Δ, Φ,... for $\Lambda = 1, 2, 3, 4 \cdots$, respectively. If the electronic wavefunction is even (gerade in German) under parity it is shown by the symbol g and if it is odd (ungerade) it is shown by the symbol u. For the Σ states, i.e. $\Lambda = 0$, there is another symmetry, which is the reflection along an arbitrary plane containing the internuclear axis. If the wavefunction is symmetric upon reflection it is shown by a $+$ sign and if it is anti-symmetric it is shown by a $-$ sign.

The number of degenerate states (with spin-orbit coupling ignored) are:

$$(2S + 1) \times 2 \ \ \text{if} \Lambda \neq 0$$
$$(2S + 1) \ \ \ \text{if} \Lambda = 0 \qquad (A2)$$

The ground state is usually shown by the letter X, and the excited states by A, B, C, ...

In this paper we are mainly dealing with the ground electronic state of the hydrogen molecule, $X^1\Sigma_g^+$, and the first three (bound) excited electronic states, $B^1\Sigma_u^+$ and $C^{\pm\,1}\Pi_u$. The $C^{\pm}$ states have different parities under the exchange of the two nuclei, as will be explained in more detail in the next appendix.

Appendix B: Formulae for H_2 dipole transitions

This appendix summarizes the notation and formulae we use for the H_2 molecular wave function and the dipole transition rates.

We use unprimed coordinates (x, y, z) to denote a laboratory-fixed frame, and primed (x', y', z') to denote a coordinate system that rotates with the molecule: the z'-axis is taken to be parallel to the internuclear separation vector $\mathbf{R}$, and the x' axis is then chosen to lie in the zz'-plane.

We use the Born-Oppenheimer (BO) approximation to solve the Schroedinger equation for the hydrogen molecule. In this approximation instead of solving one partial differential equation for a wavefunction depending on 12 variables (3 for each particle) it is separated into two partial differential equations, one for protons and one for electrons. The success of this separation is due to the large mass of the protons compared to electron. One can then assume that the protons are moving so slowly that we can solve the wavefunction of the electrons assuming the protons are at a *fixed* separation R. One also finds the eigenvalues of this equation, $E_e(R)$, which then serve as the potential in the Schroedinger equation for the protons. The criterion for this approximation to be valid is that the energy difference between the electronic energy levels is large enough so that the approximation of the adiabaticity is valid, i.e. the electrons do not jump from one quantum state to another as the protons move. Since Σ states are non-degenerate the application of the BO approximation for them is straightforward. In the case of Π electronic states, however, we need to consider the two degenerate states, with opposite angular momentum along the internuclear axis, simultaneously. Here, we present the outline of the calculation for the Π states after which it will be clear how to change the result for the Σ states.

For the Π electronic states the total wavefunction can be separated as:

$$\Psi(\mathbf{r}, \mathbf{R}) = \Phi_+(\mathbf{R})\chi_+(\mathbf{r}|\mathbf{R}) + \Phi_-(\mathbf{R})\chi_-(\mathbf{r}|\mathbf{R}) \qquad (B1)$$

where $\mathbf{r} = \mathbf{r_1}, \mathbf{r_2}$ are the positions of the two electrons and $\mathbf{R}$ the internuclear separation vector. Also, $\chi_\pm$ are the solutions of the electronic part of the Schroedinger equation:

$$\left(-\frac{1}{2m_e}\nabla_{\mathbf{r_1}}^2 - \frac{1}{2m_e}\nabla_{\mathbf{r_2}}^2 + V(\mathbf{r}_1, \mathbf{r}_2, \mathbf{R})\right)\chi_\pm(\mathbf{r}_1, \mathbf{r}_2|\mathbf{R})$$
$$= E_e(R)\chi_\pm(\mathbf{r}_1, \mathbf{r}_2|\mathbf{R}) \qquad (B2)$$

and with angular momentum along the internuclear axis of

$$\left(\mathbf{L}.\hat{\mathbf{R}}\right)\chi_\pm = \pm\chi_\pm \qquad (B3)$$

where V in equation (B2) is the sum of the potential energy among all the particles:

$$V(\mathbf{r}_1, \mathbf{r}_2, \mathbf{R}) = \frac{e^2}{R^2} - \frac{e^2}{|\mathbf{r}_1 - \frac{\mathbf{R}}{2}|^2} - \frac{e^2}{|\mathbf{r}_2 - \frac{\mathbf{R}}{2}|^2}$$
$$- \frac{e^2}{|\mathbf{r}_1 + \frac{\mathbf{R}}{2}|^2} - \frac{e^2}{|\mathbf{r}_2 + \frac{\mathbf{R}}{2}|^2} + \frac{e^2}{|\mathbf{r}_1 - \mathbf{r}_2|^2} \qquad (B4)$$

The action of the internuclear momentum operator on $\chi_\pm$ can be written as:

$$\nabla_{\mathbf{R}}\chi_+ = \vec{a}_{++}\chi_+ + \vec{a}_{+-}\chi_-$$
$$\nabla_{\mathbf{R}}\chi_- = \vec{a}_{-+}\chi_+ + \vec{a}_{-+}\chi_- \qquad (B5)$$

They are found by evaluating the following integrals:

$$\vec{a}_{\pm\pm} = \int d\mathbf{r}\chi_\pm^*(\mathbf{r}|\mathbf{R})\nabla_{\mathbf{R}}\chi_\pm(\mathbf{r}|\mathbf{R}) \qquad (B6)$$

By going to the frame of reference rotating with the whole molecule one can show that:

$$\vec{a}_{+-} = \vec{a}_{-+} = 0 \quad \vec{a}_{++} = -\vec{a}_{--} = -\frac{i}{R}\cot(\theta)\hat{e}_\phi \quad (B7)$$

Plugging equation B1 into the Schroedinger equation

$$\left(-\frac{1}{2\mu}\nabla_{\mathbf{R}}^2 - \frac{1}{2m_e}\nabla_{\mathbf{r_1}}^2 - \frac{1}{2m_e}\nabla_{\mathbf{r_2}}^2 + V(\mathbf{r}_1, \mathbf{r}_2, \mathbf{R})\right)\Psi(\mathbf{r}, \mathbf{R})$$
$$= E_{tot}\Psi(\mathbf{r}, \mathbf{R}) \qquad (B8)$$

and using equations (B5) and (B7) we find the partial differential equation for the nuclear (vibrational+rotational) part of the wavefunction as:

$$\left[-\frac{1}{2\mu}\left(\nabla^2_{\mathbf{R}} \mp \frac{2i}{R^2}\frac{\cot(\theta)}{\sin(\theta)}\frac{\partial}{\partial\phi} - \frac{1}{R^2}\cot^2(\theta)\right) + E_e(R)\right]\Phi_\pm(\mathbf{R})$$
$$= E_{tot}\Phi_\pm(\mathbf{R}) \qquad (B9)$$

For the Σ electronic states one finds a similar equation but without the terms containing $\cot(\theta)$. The usual trick of separating the radial and angular parts of the wave function results in

$$\Phi_\pm(\mathbf{R}) = \frac{\phi_{\nu J}(R)}{R}Y^{\pm 1}_{JM}(\hat{\mathbf{R}}) \qquad (B10)$$

where Y^s_{JM} is a spin-s spherical harmonic [83, 84]. (Some references, e.g. Ref. [70], use rotation matrices instead of spin-weighted spherical harmonics, but these are equivalent.) . Also, ν is the nuclear vibrational quantum number and J and M are the total and z direction (of the fixed laboratory frame) angular momentum quantum numbers of the nuclei. For any given J, different vibrational levels can be found as the eigenfunctions of the following equation:

$$\left[-\frac{1}{2\mu}\frac{d^2}{dR^2} + E_e(R) + \frac{J(J+1)-1}{2\mu R^2}\right]\phi_{J\nu}(R) = E_{\nu J}\phi_{\nu J}(R) \qquad (B11)$$

The corresponding equation for the Σ electronic states is the same except that the effective angular momentum potential is $J(J+1)/2\mu R^2$ instead. We solve the above equation, and the one for the Σ electronic states, numerically to find all the vibrational and rotational wavefunctions and energy levels of H_2 molecules in C, B and X electronic states. We use the values of $E_e(R)$ for the X,B and C electronic state calculated by [71], [72] and [73] respectively.

Since the dipole transitions are allowed for transitions with initial and final states of opposite parity it is appropriate to construct a linear combination of the nuclear wavefunctions so they become the eigenstates of the parity operator. They are called C^+ and C^- states and are given as:

$$\Psi_{C^\pm,\nu JM}(\mathbf{r},\mathbf{R}) = \frac{\phi_{\nu J}(R)}{\sqrt{2}R}\left[Y^{+1}_{JM}(\hat{\mathbf{R}})\chi_+(\mathbf{r}|\mathbf{R})\right.$$
$$\left. \pm Y^{-1}_{JM}(\hat{\mathbf{R}})\chi_-(\mathbf{r}|\mathbf{R})\right], \qquad (B12)$$

which are degenerate (Λ-doubled) in our level of approximation.

Normalization of the total wavefunction then requires $\int_0^\infty |\phi_{\nu J}(R)|^2 dR = 1$. Since the C electronic states have parity u, i.e. $\chi(-\mathbf{r}|\mathbf{R}) = -\chi(\mathbf{r}|\mathbf{R})$, the total wavefunction satisfies: $\Psi_{C^\pm,\nu JM}(\mathbf{r},-\mathbf{R}) = \pm(-1)^{J+1}\Psi_{C^\pm,\nu JM}(\mathbf{r},\mathbf{R})$.

The Einstein coefficients for dipole transitions are discussed in general textbooks, e.g. Refs. [85, 86]. In our case, the C$\rightarrow$X transition rates are as follows: for the electric dipole transition of a H_2 molecule from an excited state $a = (C,\nu_a,J_a)$ to a lower level $b = (X,\nu_b,J_b)$,

we have

$$A_{ab} = \frac{4e^2(E_a-E_b)^3}{3\hbar^4 c^3(2J_a+1)}|\mathcal{M}_{ab}|^2, \qquad (B13)$$

where the matrix element is

$$|\mathcal{M}_{ab}|^2 = \sum_{M_a=-J_a}^{J_a}\sum_{M_b=-J_b}^{J_b}|\langle\Psi_{X\nu_b J_b M_b}|\mathbf{d}|\Psi_{C\nu_a J_a M_a}\rangle|^2. \qquad (B14)$$

Here $\mathbf{d} = -e\mathbf{r}_1 - e\mathbf{r}_2$ is the electric dipole operator. The matrix element expands as

$$\langle\Psi_{X\nu_b J_b M_b}|\mathbf{d}|\Psi_{C^\pm\nu_a J_a M_a}\rangle$$
$$= \int d^3\mathbf{R}\frac{\phi^*_{X\nu_b J_b}(R)}{R}\frac{\phi_{C\nu_a J_a}(R)}{\sqrt{2}R}Y^*_{J_b M_b}(\hat{\mathbf{R}})$$
$$\times\left[Y^{+1}_{J_a M_a}(\hat{\mathbf{R}})\mathbf{D}^{CX}_+(\mathbf{R}) \pm Y^{-1}_{J_a M_a}(\hat{\mathbf{R}})\mathbf{D}^{CX}_-(\mathbf{R})\right], (B15)$$

where the fixed-$\mathbf{R}$ electric dipole moment for the $C\rightarrow X$ transition is:

$$\mathbf{D}^{CX}_\pm(\mathbf{R}) = -e\int d\mathbf{r}^3_1 d\mathbf{r}^3_2\chi^*_X(\mathbf{r}|\mathbf{R})(\mathbf{r}_1+\mathbf{r}_2)\chi_{C,\pm}(\mathbf{r}|\mathbf{R})$$
$$= D_{CX}(R)\frac{-\hat{\mathbf{x}}'\pm i\hat{\mathbf{y}}'}{\sqrt{2}}. \qquad (B16)$$

The values of $D_{CX}(R)$ are calculated in [73]. For the B$\rightarrow$X transition one finds $\mathbf{D}^{BX}(\mathbf{R}) = D_{BX}(R)\hat{\mathbf{R}}$. We use the results of [74] for it.

By plugging Eq. (B16) into Eq. (B15), separating the R integration from the $\hat{\mathbf{R}}$ integration, writing $\hat{\mathbf{x}}'$ and $\hat{\mathbf{y}}'$ in terms of the fixed coordinated unit vectors ($\hat{\mathbf{x}}$,$\hat{\mathbf{y}}$,$\hat{\mathbf{z}}$) with coefficient written in the form of spin weighted spherical harmonics with degree $s = 0$, calculating the integrals of the three spin-weighted spherical harmonics in terms of the Wigner $3j$ symbols and using the orthogonality relations of the $3j$ symbols to do the sums over M_a and M_b one finally finds:

$$|\mathcal{M}^P_{ab}|^2 = J_a K(C^+\nu_a J_a, X\nu_b J_b),$$
$$|\mathcal{M}^R_{ab}|^2 = (J_a+1)K(C^+\nu_a J_a, X\nu_b J_b), \text{ and}$$
$$|\mathcal{M}^Q_{ab}|^2 = (2J_a+1)K(C^-\nu_a J_a, X\nu_b J_b), \qquad (B17)$$

where the change in angular momentum is denoted by the branch indices P ($J_b - J_a = 1$), Q ($J_b - J_a = 0$), and R ($J_b - J_a = -1$), and

$$K(Y_a\nu_a J_a, Y_b\nu_b J_b)$$
$$= \left|\int_0^\infty\phi^*_{Y_b\nu_b J_b}(R)D_{AB}(R)\phi_{Y_a\nu_a J_a}(R)dR\right|^2. (B18)$$

Similarly, for the B$\rightarrow$X transitions,

$$|\mathcal{M}^P_{ab}|^2 = (J_a+1)K(B\nu_a J_a, X\nu_b J_b) \text{ and}$$
$$|\mathcal{M}^R_{ab}|^2 = J_a K(B\nu_a J_a, X\nu_b J_b). \qquad (B19)$$

These equations agree with Ref. [70], appropriately restricted to the case of no B–C mixing.

[1] C. L. Bennett *et al.*, ApJS**148**, 1 (2003), arXiv:astro-ph/0302207.
[2] G. Jungman, M. Kamionkowski, A. Kosowsky, and D. N. Spergel, Phys. Rev. D**54**, 1332 (1996), arXiv:astro-ph/9512139.
[3] P. J. E. Peebles and J. T. Yu, ApJ**162**, 815 (1970).
[4] J. M. Bardeen, Phys. Rev. D**22**, 1882 (1980).
[5] J. R. Bond and A. S. Szalay, ApJ**274**, 443 (1983).
[6] U. Seljak, N. Sugiyama, M. White, and M. Zaldarriaga, Phys. Rev. D**68**, 083507 (2003), arXiv:astro-ph/0306052.
[7] P. J. E. Peebles, ApJ**153**, 1 (1968).
[8] Y. B. Zeldovich, V. G. Kurt, and R. A. Syunyaev, Zhurnal Eksperimental noi i Teoreticheskoi Fiziki **55**, 278 (1968).
[9] T. Matsuda, H. Satō, and H. Takeda, Progress of Theoretical Physics **42**, 219 (1969).
[10] T. Matsuda, H. Sato, and H. Takeda, Progress of Theoretical Physics **46**, 416 (1971).
[11] W. Hu, D. Scott, N. Sugiyama, and M. White, Phys. Rev. D**52**, 5498 (1995), arXiv:astro-ph/9505043.
[12] V. K. Dubrovich and S. I. Grachev, Astronomy Letters **31**, 359 (2005).
[13] E. E. Kholupenko, A. V. Ivanchik, and D. A. Varshalovich, MNRAS**378**, L39 (2007), arXiv:astro-ph/0703438.
[14] E. R. Switzer and C. M. Hirata, Phys. Rev. D**77**, 083006 (2008), arXiv:astro-ph/0702143.
[15] C. M. Hirata and E. R. Switzer, Phys. Rev. D**77**, 083007 (2008), arXiv:astro-ph/0702144.
[16] E. R. Switzer and C. M. Hirata, Phys. Rev. D**77**, 083008 (2008), arXiv:astro-ph/0702145.
[17] J. A. Rubiño-Martín, J. Chluba, and R. A. Sunyaev, A&A**485**, 377 (2008), 0711.0594.
[18] J. Chluba and R. A. Sunyaev, MNRAS**402**, 1221 (2010), 0909.2378.
[19] J. Chluba, J. A. Rubiño-Martín, and R. A. Sunyaev, MNRAS**374**, 1310 (2007), arXiv:astro-ph/0608242.
[20] D. Grin and C. M. Hirata, Phys. Rev. D**81**, 083005 (2010), 0911.1359.
[21] J. Chluba, G. M. Vasil, and L. J. Dursi, MNRAS**407**, 599 (2010), 1003.4928.
[22] S. de, E. Baron, and P. H. Hauschildt, MNRAS**407**, 658 (2010), 1005.0580.
[23] Y. Ali-Haïmoud and C. M. Hirata, Phys. Rev. D**82**, 063521 (2010), 1006.1355.
[24] J. Chluba and R. A. Sunyaev, A&A**446**, 39 (2006), arXiv:astro-ph/0508144.
[25] E. E. Kholupenko and A. V. Ivanchik, Astronomy Letters **32**, 795 (2006), arXiv:astro-ph/0611395.
[26] W. Y. Wong and D. Scott, MNRAS**375**, 1441 (2007), arXiv:astro-ph/0610691.
[27] J. Chluba and R. A. Sunyaev, A&A**480**, 629 (2008), 0705.3033.
[28] C. M. Hirata, Phys. Rev. D**78**, 023001 (2008), 0803.0808.
[29] J. Chluba and R. A. Sunyaev, A&A**512**, A53+ (2010), 0904.0460.
[30] J. H. Krolik, ApJ**338**, 594 (1989).
[31] J. H. Krolik, ApJ**353**, 21 (1990).
[32] S. I. Grachev and V. K. Dubrovich, Astrophysics **34**, 124 (1991).
[33] G. B. Rybicki and I. P. dell'Antonio, ApJ**427**, 603 (1994),
[34] S. I. Grachev and V. K. Dubrovich, Astronomy Letters **34**, 439 (2008), 0801.3347.
[35] J. Chluba and R. A. Sunyaev, A&A**496**, 619 (2009), 0810.1045.
[36] C. M. Hirata and J. Forbes, Phys. Rev. D**80**, 023001 (2009), 0903.4925.
[37] J. Chluba and R. A. Sunyaev, A&A**503**, 345 (2009), 0904.2220.
[38] J. Chluba and R. A. Sunyaev, A&A**475**, 109 (2007), arXiv:astro-ph/0702531.
[39] E. E. Kholupenko, A. V. Ivanchik, and D. A. Varshalovich, Phys. Rev. D**81**, 083004 (2010), 0912.5454.
[40] S. Seager, D. D. Sasselov, and D. Scott, ApJ**523**, L1 (1999), arXiv:astro-ph/9909275.
[41] S. Seager, D. D. Sasselov, and D. Scott, ApJS**128**, 407 (2000), arXiv:astro-ph/9912182.
[42] W. Y. Wong, A. Moss, and D. Scott, MNRAS**386**, 1023 (2008), 0711.1357.
[43] A. Lewis, J. Weller, and R. Battye, MNRAS**373**, 561 (2006), arXiv:astro-ph/0606552.
[44] J. Chluba and R. M. Thomas, ArXiv e-prints (2010), 1010.3631.
[45] Y. Ali-Haïmoud and C. M. Hirata, ArXiv e-prints (2010), 1011.3758.
[46] D. Galli and F. Palla, A&A**335**, 403 (1998), arXiv:astro-ph/9803315.
[47] D. R. G. Schleicher *et al.*, A&A**490**, 521 (2008), 0803.3987.
[48] W. C. Saslaw and D. Zipoy, Nature**216**, 976 (1967).
[49] P. J. E. Peebles and R. H. Dicke, ApJ**154**, 891 (1968).
[50] T. Hirasawa, K. Aizu, and M. Taketani, Progress of Theoretical Physics **41**, 835 (1969).
[51] T. Yoneyama, PASJ**24**, 87 (1972).
[52] J. B. Hutchins, ApJ**205**, 103 (1976).
[53] S. Lepp and J. M. Shull, ApJ**280**, 465 (1984).
[54] Z. Haiman, A. A. Thoul, and A. Loeb, ApJ**464**, 523 (1996), arXiv:astro-ph/9507111.
[55] Z. Haiman, M. J. Rees, and A. Loeb, ApJ**467**, 522 (1996), arXiv:astro-ph/9511126.
[56] M. Tegmark *et al.*, ApJ**474**, 1 (1997), arXiv:astro-ph/9603007.
[57] P. C. Stancil, S. Lepp, and A. Dalgarno, ApJ**509**, 1 (1998).
[58] D. R. Flower and G. Pineau des Forêts, MNRAS**316**, 901 (2000).
[59] S. Lepp, P. C. Stancil, and A. Dalgarno, Journal of Physics B Atomic Molecular Physics **35**, 57 (2002).
[60] C. M. Hirata and N. Padmanabhan, MNRAS**372**, 1175 (2006), arXiv:astro-ph/0606437.
[61] J. Chluba and R. A. Sunyaev, A&A**458**, L29 (2006), arXiv:astro-ph/0608120.
[62] J. Chluba and R. A. Sunyaev, A&A**488**, 861 (2008), 0804.1017.
[63] S. C. Glover, D. W. Savin, and A. Jappsen, ApJ**640**, 553 (2006), arXiv:astro-ph/0506221.
[64] S. C. O. Glover and T. Abel, MNRAS**388**, 1627 (2008), 0803.1768.
[65] S. C. O. Glover and D. W. Savin, MNRAS**393**, 911 (2009), 0809.0780.
[66] A. Dalgarno and M. P. J. van der Loo, ApJ**646**, L91

arXiv:astro-ph/9312006.

(2006).

[67] V. V. Sobolev, Soviet Ast. **1**, 678 (1957).

[68] V. V. Sobolev, *Moving envelopes of stars* (, 1960).

[69] H. Abgrall, E. Roueff, and I. Drira, A&AS **141**, 297 (2000).

[70] H. Abgrall and E. Roueff, A&AS **79**, 313 (1989).

[71] L. Wolniewicz, J. Chem. Phys. **99**, 1851 (1993).

[72] G. Staszewska and L. Wolniewicz, Journal of Molecular Spectroscopy **212**, 208 (2002).

[73] L. Wolniewicz and G. Staszewska, Journal of Molecular Spectroscopy **220**, 45 (2003).

[74] L. Wolniewicz and G. Staszewska, Journal of Molecular Spectroscopy **217**, 181 (2003).

[75] W. H. Press, S. A. Teukolsky, W. T. Vetterling, and B. P. Flannery, *Numerical recipes in C. The art of scientific computing* (, 1992).

[76] L. Wolniewicz, I. Simbotin, and A. Dalgarno, ApJS **115**, 293 (1998).

[77] P. S. Krstić, Phys. Rev. A **66**, 042717 (2002).

[78] Z. Karpas, V. Anicich, and W. T. Huntress, J. Chem. Phys. **70**, 2877 (1979).

[79] V. M. Andrianarijaona, J. J. Rada, R. Rejoub, and C. C. Havener, Journal of Physics Conference Series **194**, 012043 (2009).

[80] J. M. Launay, M. Le Dourneuf, and C. J. Zeippen, A&A **252**, 842 (1991).

[81] D. Fussen and C. Kubach, Journal of Physics B Atomic Molecular Physics **19**, L31 (1986).

[82] I. F. Schneider, O. Dulieu, A. Giusti-Suzor, and E. Roueff, ApJ **424**, 983 (1994).

[83] E. T. Newman and R. Penrose, Journal of Mathematical Physics **7**, 863 (1966).

[84] J. N. Goldberg, A. J. Macfarlane, E. T. Newman, F. Rohrlich, and E. C. G. Sudarshan, Journal of Mathematical Physics **8**, 2155 (1967).

[85] L. D. Landau and E. M. Lifshitz, *Quantum mechanics* (, 1965).

[86] V. B. Berestetskii, E. M. Lifshits, and L. P. Pitaevskii, Moscow Izdatel Nauka Teoreticheskaia Fizika **4** (1980).